Unified closed-form model of thermionic-field and field emissions through a triangular potential barrier

Shreepad Karmalkar and D. Mahaveer Sathaiya

Citation: Applied Physics Letters **82**, 1431 (2003); doi: 10.1063/1.1557773
View online: http://dx.doi.org/10.1063/1.1557773
View Table of Contents: http://scitation.aip.org/content/aip/journal/apl/82/9?ver=pdfcov
Published by the AIP Publishing

Unified closed-form model of thermionic-field and field emissions through a triangular potential barrier

Shreepad Karmalkar[a] and D. Mahaveer Sathaiya
Department of Electrical Engineering, Indian Institute of Technology, Madras 600 036, India

(Received 11 October 2002; accepted 8 January 2003)

We report a simple closed-form model of the *total* emission *through* a triangular potential barrier due to thermionic field emission (TFE) and field emission (FE). Such a model has not been derived previously, since the energy distribution function of emitted electrons is not analytically integrable. We overcame this difficulty using a geometrical approximation of the integration operation. Our model so derived reveals the energy location and spread of the emission, which allow estimation of the emission through any fraction of the barrier. It also yields a characteristic field parameter in terms of the barrier height, temperature, and effective mass, which can be used to identify the TFE, FE, and TE regimes of device operation. © *2003 American Institute of Physics.*
[DOI: 10.1063/1.1557773]

Electron current flows by thermionic emission (TE) across interfaces in several modern electronic devices. As the size of these devices, and the films used therein, shrink progressively, the interface electric fields shoot up, activating thermionic-field emission (TFE), and pure field emission (FE) currents *through* the interface potential barrier, which begin to dominate the TE current *over* the barrier. The interface potential barrier is often well approximated by a triangular shape (see Fig. 1). A simple closed-form model is available for FE through such a barrier, but not for TFE, forcing the need for numerical techniques to determine the *total* emission. This has been an impediment in the design, analysis and parameter extraction of several modern devices having metal–vacuum, Schottky, MIS, and heterointerfaces, planar doped barriers, carbon nanotubes, and quantum dots, wherein the TFE and FE emission is important.[1–10]

In this letter, we derive a simple closed-form model of the *total* emission, including the TFE, through a triangular barrier. The model follows a smooth gradation between the extremes of pure TE and pure FE via TFE. It reveals the energy location and spread of the emission, enabling estimation of the emission through a portion of the barrier height as required in many situations, e.g., in the emitter heterojunction in a *pnp* HBT, where the potential drop associated with the barrier electric field is less than the barrier height.[4]

The total emitted current density through the barrier due to TFE and FE (see Fig. 1) can be written as

$$J = q^2 \int_{-\phi_F}^{\phi_B} \nu_x(\phi) N(\phi) f_{\mathrm{FD}}(\phi) \Gamma(\phi) d\phi, \tag{1}$$

where, $\nu_x(\phi)$ is the electron velocity directed against the barrier, $N(\phi)$ is the density of states, and $f_{\mathrm{FD}}(\phi)$ is the Fermi–Dirac function (assumed to be zero on the right-hand side of the barrier), and $\Gamma(\phi)$ is the quantum mechanical transmission coefficient; ϕ is in volts. The behavior of J as a function of the temperature, T, and electric field, E, is strongly governed by $f_{\mathrm{FD}}(\phi)$ and $\Gamma(\phi)$:

$$f_{\mathrm{FD}}(\phi) = \frac{1}{1+\exp(\phi/V_t)}, \quad \Gamma(\phi) = \exp\left[-\frac{\alpha}{E}(\phi_B - \phi)^{3/2}\right],$$

$$\alpha = \frac{8\pi\sqrt{2mq}}{3h}, \tag{2}$$

where $\Gamma(\phi)$ is based on the WKB approximation, m is the electron effective mass, and other symbols have their usual meanings. Hence, the term $[q^2 \nu_x(\phi) N(\phi)]$ in Eq. (1), can be effectively treated as a constant, θ, and we can write

$$J \approx \theta \int_{-\phi_F}^{\phi_B} Z(\phi) d\phi,$$

$$Z(\phi) = \frac{1}{\left[1+\exp\frac{\phi}{V_t}\right]\exp\left[\frac{\alpha}{E}(\phi_B-\phi)^{3/2}\right]}. \tag{3}$$

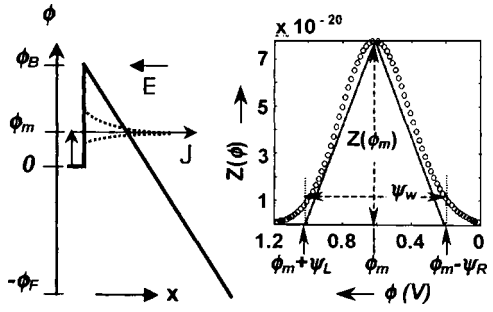

FIG. 1. Showing a triangular potential barrier (height ϕ_B, thick solid line), and the critical energy levels, namely, the Fermi level ($\phi = 0$), the conduction band minimum ($\phi = -\phi_F$), and the energy location of maximum emission ($\phi = \phi_m$), all on the left-hand side of the barrier. Also shown is the numerically calculated (circles) and modeled (solid lines) shape of the energy distribution of emitted electrons [Eqs. (8) and (12)], for $E = 0.75\,E_0 = 1.13$ MV/cm, $\phi_B = 1.4$ V, $T = 300$ K.

[a]Electronic mail: skarmalkar@hotmail.com

The function $Z(\phi)$ is not analytically integrable, and this is why a closed-form expression for emission through a triangular barrier has not been derived previously. We overcome this difficulty and achieve other benefits, as follows. We invoke a geometrical interpretation of the integration operation, and regard the integral in Eq. (3) as the area under $Z(\phi)$ vs ϕ curve. We note from the shape of $Z(\phi)$ that this area is well approximated by a triangle (see Fig. 1). The height of the triangle is $Z(\phi_m)$, which is the peak value of $Z(\phi)$ located at $\phi=\phi_m$, and the base of the triangle is $\psi_W=\psi_L+\psi_R$, which represents the emission width, and is obtained using the condition $Z(\phi_m+\Psi_L)=Z(\phi_m-\Psi_R)=Z(\phi_m)/e^2$. Thus, we write

$$\int_{-\phi_F}^{\phi_B} Z(\phi)d\phi \approx \frac{1}{2}\psi_w Z(\phi_m). \tag{4}$$

As will be shown below, it is possible to provide simple closed-form expressions for the parameters namely—ϕ_m, ψ_W, ψ_L, ψ_R, and $Z(\phi_m)$. The great advantage of this is that, all features of the triangular distribution, namely its location, height, and spread on either side of the peak (even if asymmetric) are revealed in terms of simple expressions of the various physical variables, which in turn allows estimation of the integral term on the LHS of Eq. (4) between *any pair* of potential limits (and not just $-\phi_F$ and ϕ_B).

Once the integral in Eq. (3) is obtained from Eq. (4), an expression for θ is derived using the condition that, at $T\rightarrow 0$, the J obtained from Eq. (3) should correspond to the Fowler–Nordheim current (numerator of the equation below):[11]

$$\theta=\frac{\dfrac{q^2E^2}{8\pi h\phi_B}\exp(-\alpha\phi_B^{3/2}/E)}{0.5\psi_w Z(\phi_m)|_{T\rightarrow 0}}. \tag{5}$$

The expressions for ϕ_m, ψ_W, ψ_L, ψ_R, and $Z(\phi_m)$ are now derived. Differentiating the denominator of $Z(\phi)$ in Eq. (3), and setting it to zero yields

$$\frac{\phi_m}{\phi_B}=1-\left\{\frac{E/E_0}{1+\exp(-\phi_m/V_t)}\right\}^2,\quad E_0=1.5\alpha V_t\sqrt{\phi_B}. \tag{6}$$

As will be shown, E_0 is a characteristic field, in terms of which the TFE, FE, and TE dominated regimes of operation can be identified. From Eq. (6), ϕ_m can be solved iteratively. However, without loss of accuracy, significant simplification and physical insight are gained by the following approximation of Eq. (6), illustrated in Fig. 2(a):

$$(\phi_m/\phi_B)\approx\{1-(E/E_0)^2\}\ \text{ for }\ E\leqslant E_0,$$
$$\phi_m\approx 0\ \text{ for }\ E>E_0. \tag{7}$$

Using this and $\exp(\phi_m/V_t)\gg 1$ in Eq. (3), we obtain [see Fig. 2(b)]:

$$Z(\phi_m)\approx \exp-\left\{\frac{\phi_B}{V_t}\left[1-\frac{1}{3}\left(\frac{E}{E_0}\right)^2\right]\right\}\ \text{ for }\ E\leqslant E_0, \tag{8}$$

$$Z(\phi_m)\approx \exp-\left(\frac{\alpha\phi_B^{3/2}}{E}\right)\ \text{ for }\ E>E_0. \tag{9}$$

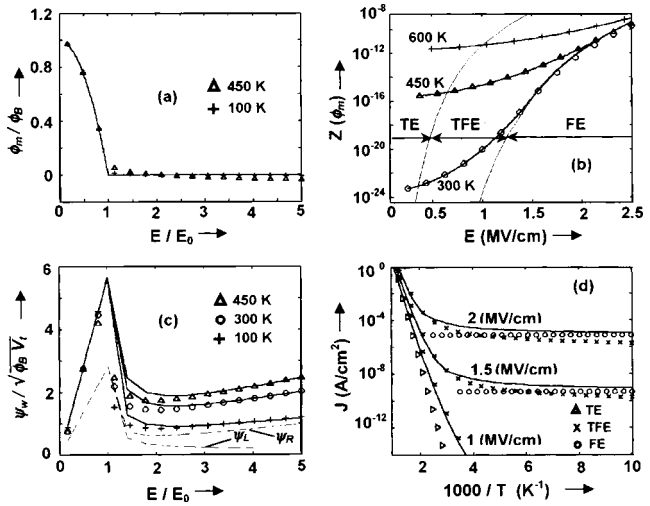

FIG. 2. Comparison of numerical calculations (points) with our model (lines), using $\phi_B=1.4$ V, $m=0.23\,m_0$: (a) normalized energy location of the maximum emission [Eq. (6)]; (b) maximum emission expressed in terms of the maximum of $Z(\phi)$ [Eqs. (8) and (9)]; (c) the normalized energy spread of emission [Eqs. (12)–(14)]. Also shown are the components ψ_L and ψ_R of this spread at 100 K; (d) the total emitted electron current [Eqs. (3), (4), (8), (9), (12)–(15)] and the numerically calculated FE, TFE, and TE segments using standard formulas (Refs. 2 and 11).

Strictly speaking, $\exp(\phi_m/V_t)$ is not $\gg 1$ if $\phi_m\approx 0$ is used for $E>E_0$. However, this approximation has been used to maintain continuity in $Z(\phi_m)$ at $E=E_0$.

Expressions for ψ_R, ψ_L, and $\psi_W=\psi_R+\psi_L$ are derived by solving $Z(\phi_m+\psi_L)=e^{-2}Z(\phi_m)=Z(\phi_m-\psi_R)$. For $E\leqslant E_0$, using $\exp(\phi_m/V_t)\gg 1$ and $\exp[(\phi_m+\psi_L)/V_t]\gg 1$ in $Z(\phi_m+\psi_L)=e^{-2}Z(\phi_m)$, and taking logarithms, we obtain

$$\frac{\psi_L}{V_t}+\frac{\alpha}{E}(\phi_B-\phi_m)^{3/2}\left\{\left(1-\frac{\psi_L}{\phi_B-\phi_m}\right)^{3/2}-1\right\}\approx 2, \tag{10}$$

which can be further simplified, using $[\psi_L/(\phi_B-\phi_m)]\ll 1$ and $(1-x)^{3/2}\approx[1-(3/2)x+(3/8)x^2]$ for $x\ll 1$, to

$$\psi_L\left(\frac{1}{V_t}-\frac{3\alpha\sqrt{\phi_B-\phi_m}}{2E}\right)+\frac{3}{8}\frac{\alpha}{E}\left(\frac{\psi_L^2}{\sqrt{\phi_B-\phi_m}}\right)\approx 2. \tag{11}$$

Based on Eq. (7), the first term of this equation is ≈ 0, since $(E/E_0)<1$. A similar approach is used to derive ψ_R using $\exp[(\phi_m-\psi_R)/V_t]\gg 1$ and $[\psi_R/(\phi_B-\phi_m)]\ll 1$. The result is a common expression for ψ_L and ψ_R;

$$\psi_L\approx\psi_R\approx 2\sqrt{2}\sqrt{\phi_B V_t}\left(\frac{E}{E_0}\right)\quad \text{for}\ E\ll E_0. \tag{12}$$

For $(E/E_0)>1$, ψ_L and ψ_R behave differently for large (E/E_0), or equivalently, small T, and their solutions should be considered separately. For $T\rightarrow 0$, thermal activation is disabled and only pure FE exists, the emission distribution $Z(\phi)$ shows a maximum at $\phi=0$, a steep fall for $\phi>0$ and a relatively slow decay for $\phi<0$, implying ψ_L tends to zero but ψ_R does not. In fact, ψ_R increases linearly for large (E/E_0). This is seen by solving for ψ_R from $Z(\phi_m-\psi_R)=e^{-2}Z(\phi_m)$ at $T\rightarrow 0$, when $f_{\mathrm{FD}}(\phi_m)=1$ [equivalently, set $\exp(\phi_m/V_t)=0$ in Eq. (3)]; using $\psi_R/\phi_B\ll 1$ and $(1+x)^{3/2}\approx[1+(3/2)x]$ for $x\ll 1$, we obtain $\psi_R\approx 2\,V_t\,(E/E_0)$. A ψ_L expression is derived as follows. Since numerical results shows $\phi_m>0$ up to $(E/E_0)=2$ [see Eq. (6) and Fig. 2(a)],

the approximations used to derive ψ_L for $(E/E_0)<1$ hold for some range of $(E/E_0)>1$ also, except that $\phi_B-\phi_m\approx\phi_B$ in this case. This yields

$$\psi_L\approx 2\phi_B\left\{\sqrt{\left(\frac{E}{E_0}-1\right)^2+2\left(\frac{V_t}{\phi_B}\right)\left(\frac{E}{E_0}\right)}-\left(\frac{E}{E_0}-1\right)\right\}\quad\text{for}\quad E>E_0. \tag{13}$$

Since $\psi_L\to 0$ as $(E/E_0)\to\infty$ in this equation, it predicts the trends for large (E/E_0) as well. As per Eqs. (12) and (13), ψ_L increases linearly from $E=0$ to $E=E_0$, and decays for $E>E_0$ [see Fig. 2(c)]. Numerical calculations indicate that, the ψ_R behavior for $E>E_0$ shows a ψ_L like fall near $(E/E_0)=1$ before the linear rise for large (E/E_0) as per $\psi_R\approx 2\,V_t\,(E/E_0)$. Interestingly, this ψ_R behavior is captured by a simple modification of Eq. (13), wherein the (E/E_0) term multiplying the $2(V_t/\phi_B)$ term is replaced by $(E/E_0)^2$ [see Fig. 2(c)]:

$$\psi_R\approx 2\phi_B\left\{\sqrt{\left(\frac{E}{E_0}-1\right)^2+2\left(\frac{V_t}{\phi_B}\right)\left(\frac{E}{E_0}\right)^2}-\left(\frac{E}{E_0}-1\right)\right\}\quad\text{for}\quad E>E_0. \tag{14}$$

The values of $\psi_W=\psi_L+\psi_R$ obtained from Eqs. (12), (13), and (14) are compared with the numerical calculations in Fig. 2(c). The agreement is good except near $E=E_0$. However, this inaccuracy has no significant effect on the $J-E$ behavior, which is dominated by the $Z(\phi_m)-E$ behavior of Eqs. (8) and (9).

Using the above facts at $T\to 0$, namely $Z(\phi_m)\approx\exp(-\alpha\phi_B^{3/2}/E)$ and $\psi_W\approx\psi_R\approx 2\,V_t\,(E/E_0)$ in Eq. (5), we derive

$$\theta=\frac{3\alpha q^2 E}{16\pi h\sqrt{\phi_B}}. \tag{15}$$

Figure 2(d) shows our model calculations using Eqs. (3), (4), (8), (9), (12)–(15), and the numerically calculated FE, TFE, and TE segments using standard formulas.[2,11] Clearly, the model follows a smooth gradation between the extremes of pure TE and pure FE via TFE. The $Z(\phi_m)$ Eqs. (8) and (9) show that, the FE regime is defined by $E\geqslant E_0$ where $J\sim\exp-(\alpha\,\phi_B^{3/2}/E)$, and the TE regime by $E\leqslant(E_0/\sqrt{\phi_B/3V_t})$ where $J\sim\exp-(\phi_B/V_t)$, so that TFE occurs for $(E_0/\sqrt{\phi_B/3V_t})<E<E_0$. Thus, our work yields a simple criterion for identifying the TE, TFE, and FE regimes based on the barrier height, temperature, electron effective mass, and electric field [see Fig. 2(b)].

The accuracy of ψ_L and ψ_R predictions near $(E/E_0)=1$ in Fig. 2(c) can be improved by incorporating correction factors in Eqs. (12), (13), and (14). Furthermore, the TFE through a portion of the barrier height[4] can be readily calculated using our triangular distribution of emitted electrons. These aspects of our work will be discussed in a separate publication, where we will also illustrate application of our model to situations covered by the classical TFE model[12,13] derived for the parabolic barrier in Schottky diodes with a long uniformly doped semiconductor region.

To conclude, we presented a simple closed-form model of the total current emitted through a triangular barrier due to TFE and FE. The model follows a smooth gradation between the extremes of pure TE and pure FE via TFE, and identifies the regimes of these mechanisms in terms of a characteristic field parameter. Our model reveals the energy location and spread of emitted electrons, providing significant insight. The model should prove very useful for the analysis of modern electronic devices.

[1] Y. L. Li, E. F. Schubert, J. W. Graff, A. Osinsky, and W. F. Schaff, Appl. Phys. Lett. **76**, 2728 (2000).
[2] E. J. Miller, X. Z. Dang, and E. T. Yu, J. Appl. Phys. **88**, 5951 (2000).
[3] T. Simlinger, H. Brech, T. Grave, and S. Selberherr, IEEE Trans. Electron Devices **44**, 700 (1997).
[4] S. Datta, K. P. Roenker, and M. M. Cahay, Solid-State Electron. **43**, 1299 (1999).
[5] R. Jones, A. Krier, K. Davidson, J.-P. N. Schmit, and J. Zawadzka, Thin Solid Films **340**, 221 (1999).
[6] J.-M. Bonard, H. Kind, T. Stockli, and L. O. Nilsson, Solid-State Electron. **45**, 893 (2001).
[7] F. A. M. Köck, J. M. Garguilo, B. Brown, and R. J. Nemanich, Diamond Relat. Mater. **11**, 774 (2002).
[8] T.-H. Ihn, T.-K. Kim, B.-Il Lee, and S. K. Joo, Microelectron. Reliab. **39**, 53 (1999).
[9] D. N. Christodoulides, A. G. Andreou, R. I. Joseph, and C. R. Westgate, Solid-State Electron. **28**, 821 (1985).
[10] C. M. Wu and E. S. Yang, Solid-State Electron. **22**, 241 (1979).
[11] A. van der Ziel, *Solid State Physical Electronics* (Prentice-Hall of India, New Delhi, 1971).
[12] F. A. Padovani and R. Stratton, Solid-State Electron. **9**, 695 (1966).
[13] E. H. Rhoderick and R. H. Williams, Metal-Semiconductor Contacts (Clarendon, Oxford, 1978).